DEUTSCHES ELEKTRONEN-SYNCHROTRON DESY

DESY 70/35
August 1970

Photoemission from the Potassium Halides in the Photon Energy Range 7 - 30 eV

by

D. Blechschmidt, M. Skibowski, and W. Steinmann
Sektion Physik der Universität München, München, Germany

2 HAMBURG 52 · NOTKESTIEG 1

Subject classification: 17; 13.1; 13.2; 22.5.2

PHOTOEMISSION FROM THE POTASSIUM HALIDES IN THE PHOTON ENERGY RANGE 7 - 30 eV [1)]

D. Blechschmidt, M. Skibowski, and W. Steinmann

Sektion Physik der Universität München, München, Germany

The spectral distribution of the photocurrent at different retarding potentials as well as the energy distribution of the photoelectrons at a fixed photon energy has been measured for all potassium halides. The synchrotron radiation of DESY was used as light source. The samples were thin films evaporated under ultra high vacuum. The threshold energy, the distance between the valence band and the K^+3p core level, and the position of the Fermi level has been determined. The onset of electron-electron scattering and the appearence of inelastically scattered electrons in the photoemission has been demonstrated. The decay of the core excitons has been investigated. The core exciton structure in the spectra of the photoyield is due to direct recombination. There is some evidence that an Auger process occurs as additional decay mechanism.

---

1) Supported by the Deutsche Forschungsgemeinschaft and the Deutsches Elektronen-Synchrotron

Die Spektralverteilung des Photostroms bei verschiedenen Retardierungspotentialen, sowie die Energieverteilung der Photoelektronen zu fester Photonenenergie wurde für alle Kaliumhalogenide gemessen. Als Lichtquelle diente die Synchrotronstrahlung von DESY. Als Proben wurden dünne, im Ultrahochvakuum aufgedampfte Schichten verwendet. Die Grenzwellenlänge, der energetische Abstand zwischen dem Valenzband und dem K^+3p-Rumpfniveau, sowie die Lage des Ferminiveaus wurden bestimmt. Der Einsatz der Elektron-Elektron-Streuung und das Auftreten von inelastisch gestreuten Elektronen in der Photoemission wurde nachgewiesen. Der Zerfall der Rumpfexzitonen wurde untersucht. Die Rumpfexzitonenstruktur in den Spektren der Photoausbeute ist auf direkte Rekombination zurückzuführen. Gewisse Anzeichen sprechen dafür, daß ein Auger Prozess als zusätzlicher Zerfallmechanismus auftritt.

1. INTRODUCTION

Investigations on the optical properties of the potassium halides have recently been extended to photon energies beyond 12 eV /1/-/9/. The most prominent structures of the optical spectra have been interpreted as exciton excitations from the valence band filled by the outermost electrons of the halogen ion and the core level formed by 3p states of the potassium ion. (Fig.1).

More information can be obtained from photoemission studies than from optical spectra since they allow the determination not merely of the transition energies but also of the position of the energy levels. This, however, requires an energy analysis of the photoelectrons. On the other hand, photoemission is a rather complicated process, and detailed investigation of such effects as electron scattering and other secondary processes is necessary in order to interpret the results correctly.

Photoemission studies on potassium halides have, so far, been much less complete and extensive than optical investigations. Valence band excitations have been studied by measuring the energy distribution of photoelectrons /13/, /14/. In the higher energy range, which includes the core excitations, only the photoelectric yield has been measured /7/, /10/, except for one investigation on KCl where retarding potential measurements for eight distinct photon energies in the range 10 - 50 eV have been performed /12/.

These results have lead to a tentative interpretation of the yield spectra. They show two broad maxima. A fine structure is superimposed which, for the most part, corresponds closely to the structure in the optical spectra. The decrease of the yield following the first maximum is explained by the onset of inelastic electron-electron scattering which becomes possible for photon energies larger than twice the band gap energy. By this process the primary photoelectron excites another valence band electron, resulting in two low energy electrons in the conduction band. It was found /7/ that the yield in the high energy range beyond the minimum approaches or even exceeds the value of one electron per absorbed photon. This indicates that both electrons can escape from the sample after scattering. The close correspondence between the fine structure of the yield and the optical spectra is not surprising, if one assumes that all structure in the optical data is due to transitions to final states above the vacuum level. This is certainly not true for some excitons. While the excitation of valence excitons can generally not be observed in the yield spectra, the K^+3p core exciton doublet at about 20 eV manifests itself quite clearly. This can only be due to a secondary process, by which the exciton energy is imparted wholly or partially to the photoemitted electron.

In this paper results of energy analysis of the photoelectrons are reported. They permit the direct determination of energy levels with respect to the vacuum level. Furthermore, they support the assumptions about electron scattering made to interpret the yield spectra. Finally they give information about the secondary processes leading to the core exciton structure

in the photoyield.

2. EXPERIMENT

The synchrotron radiation of the Deutsches Elektronen-Synchrotron DESY in Hamburg was used as a light source /16/, /17/, providing a continuous spectrum of extreme uv radiation. The incident light is monochromatized by a normal incidence monochromator in a modified Wadsworth mounting /18/. The resolution was about 3 Å (0.1 eV at 20 eV). The incident intensity was determined by a sodium salicylate coated photo-multiplier. As filter we used LiF below 12 eV to avoid second order light and Te above 25 eV to reduce stray light. A Cu-Be cathode intercepting part of the synchrotron light incident on the grating provided a reference signal.

Energy analysis of the photoelectrons was carried out in two ways: either the photocurrent per incident photon was measured as a function of the photon energy with a fixed retarding potential applied to the collector as parameter (a method specially suited to the continuum of the synchrotron radiation), or by the conventional method of measuring energy distribution curves at a fixed photon energy. They were obtained from current-voltage characteristics which were numerically differentiated by means of a digital computer.

The measurements were performed in an ultrahigh vacuum system at a pressure in the 10^{-9} Torr range /19/. The samples were prepared in situ by evaporation from tungsten boats onto

aluminum coated optical flats. Venting the system caused considerable changes in the data. The spectra and most of the energy distribution measurements were taken immediately after the evaporation. During the evaporation process the pressure in the sample chamber rose up to about 5×10^{-8} Torr. The film thickness ranged from 2000 - 5000 Å. The samples were mounted in the center of a spherical gold-coated stainless steel collector (diameter = 175 mm). The photocurrent from the sample, ranging from 10^{-15} to 10^{-11} amps, was measured with a vibrating reed electrometer. The reverse current at high retarding potential due to photoemission from the collector was less than 0.1% of the saturation current. The photocurrent saturated at a collector potential of 2 - 4 volts depending on the type of halide.

3. RESULTS AND DISCUSSION

3.1 Energy levels

By a quantitative analysis of the photoemission data the energy levels involved in the photoemission process can be determined. For this purpose it is necessary to consider the potential scheme of the emitter with respect to the collector, as shown in Fig. 2. Electron emission starts at the threshold energy $E_{TH} = E_G + E_A$. These quantities are listed in Table 1. Column 1 shows the gap energies as obtained from optical measurements. Column 2 contains our threshold values as compared to those of earlier publications. The difference between

these two columns gives the electron affinity in column 3. The values obtained for E_A are in good agreement with those published previously /20/, except for KBr where a more reliable value for E_G has meanwhile been obtained by two photon spectroscopy /21/.

Electrons which are excited by a photon with energy $\hbar\omega$ from an energy level E below the top of the valence band and which have lost energy E_S by inelastic scattering are stopped by the retarding potential U_R applied to the collector

$$U_R(\hbar\omega, E, E_S) = \hbar\omega - (E+E_S) - (\phi+\Delta) \quad ; \tag{1}$$

(cf. Fig.2). The corresponding kinetic energy is

$$E_{kin} = U_R - E_{TH} + \phi + \Delta \tag{2}$$

The stopping potential for electrons excited from the top of the valence band escaping from the sample without being inelastically scattered is determined by Eq.(1) with $E=E_S=0$. For electrons excited from the top of the K^+3p core level $E=E_{VC}$. In Fig. 3 the experimental stopping potentials for unscattered electrons excited from the valence band and the K^+3p core level are plotted as a function of photon energy for KI. They were obtained from the onset of the photocurrent in the spectra for different retarding potentials (Figs. 4, 5) as well as from the cutoff of the current voltage characteristic for different photon energies. The K^+3p-threshold was deter-

mined from the logarithm of the photocurrent as illustrated in Fig.5. Plots similar to Fig. 3 were obtained for all potassium halides. The energy separation of the two straight lines yields E_{VC} (Table 1, column 5). For KF, the onset of the core excitations could not be determined in this way, since in this case $E_G \approx E_{VC}$ and thus the core electron threshold is masked by the onset of scattered valence electrons.

The values for E_{VC} agree quite well with those obtained from the energy difference of the Γ- excitons from the valence band and from the K^+3p level assuming equal binding energies. The independent determination of E_{VC} by photoemission permits to examine the validity of this assumption. The binding energies of the valence exciton B_V and of the core exciton B_C is calculated by $B_V=E_G-E_{EXV}$ and $B_C=E_G+E_{VC}-E_{EXC}$ where E_{EXV} and E_{EXC} denote the excitation energy of the valence exciton and the core exciton. The values obtained are listed in column 6 and 7 of Table 1. Within the limits of error, the assumption of equal binding energies appears to be justified.

Extrapolation of the stopping potential line for the valence electrons yields the stopping potential U_{RO} at the threshold energy. For KI, $E_{TH}=7.3$ eV and $U_{RO}= -0.1$ eV, as indicated in Fig. 3. Inserting these values in Eq.(1) together with $E = E_S = 0$, one finds $(\phi + \Delta)=E_{TH}-U_{RO}=7.4$ eV. If one assumes that for KI the Fermi energy lies in the middle of the gap one gets $\Delta=E_G/2 = 3.15$ eV, and hence obtains $\phi = 4.25$ eV. This seems to be reasonable for the work function of an aged gold surface as compared to the earlier published value of 4.3 eV /11/. With

ϕ = 4.25 eV and the E_{TH} and U_{RO} values found for the other potassium halides one obtains Δ and the energy by which the Fermi level lies above the middle of the gap (column 8 and 9). The Fermi level shifts upwards from KI to KF indicating an increase in the density of lattice defects.

3.2 Electron scattering

An example of photoemission spectra taken for different retarding potentials is shown for KI in Fig.4. Similar results were obtained for KBr, KCl, and KF; therefore we restrict the discussion to KI. The uppermost curve in Fig.4 is the yield spectrum. The yield spectra of all potassium halides up to a photon energy of 30 eV have been published elsewhere /10/. For photon energies less than twice the energy gap E_G, the excited photoelectrons cannot be inelastically scattered by valence electrons. This leads to a steady increase of the yield from the threshold energy to the first maximum. At a photon energy $\hbar\omega = 2E_G$ electron-electron scattering becomes possible. The primary electron excites another valence band electron. This yields two electrons at the bottom of the conduction band below the vacuum level, so that the photoemission is drastically reduced. As the photon energy is increased, one and eventually both electrons will retain enough energy to escape from the sample. The high energy maximum in the yield curve ($\approx$ 25 eV) is roughly twice as high as the low energy one due to the fact that one photon yields two electrons /7/, /10/. The onset of inelastic scattering is indicated by the high density of the curves beyond $2E_G$, whereas their large distance at the high energy

side of the minimum points to the preferential emission of low energy electrons. When the retarding potential is increased, the high energy maximum decreases more rapidly than the low energy one. This shows that the percentage of low energy electrons is greater in the high energy range.

The onset of electron-electron scattering at $2E_G$ can be observed directly in the electron distribution curves. Figure 6 shows our data for KI. In this plot a maximum which is formed by unscattered electrons starting from a fixed energy level (cf. Eq. (1)) does not shift with the photon energy. Thus the maximum at $U_R - \hbar\omega = -11$ eV corresponds to the valence band; it does not move when the photon energy is increased from 10 to 11.7 eV. The width of this peak is larger than the calculated width of the valence band /22/, /24/. This broadening is caused by space charge effects. It does not affect the further conclusions we draw from the energy distribution curves. At $\hbar\omega = 13.0$ eV the photon energy just exceeds the scattering threshold. This causes a shift of the peak which is brought about by the scattering of electrons from the high energy side of the maximum. With increasing photon energy more and more scattered electrons can escape. At $\hbar\omega = 14.5$ eV two distinct peaks have developed. The high energy peak, which is caused by the unscattered electrons, is essentially unshifted. At $\hbar\omega = 15.0$ eV the number of scattered electrons is already greater than the number of the unscattered ones. This fact can be evaluated quantitatively. In Fig.7 the ratio N_S/N_V of the peak-heights of the scattered to the unscattered electrons is plotted for all potassium halides as a function of photon energy. The

double threshold energy $2(E_G+E_A)$ is marked by arrows. At this energy the ratio N_S/N_V rises steeply since the two scattered electrons can be emitted. Consequently the minimum of the photoyield (Fig.4) is expected at $2(E_G+E_A)$. In column 4 of Table 1 half of the photon energy at which the minimum occurs is listed. These values are in good agreement with the threshold energy E_G+E_A in column 2, indicating that the minimum indeed lies at $2(E_G+E_A)$ rather than at $2\ E_G+E_A$, as assumed previously /10/.

The steep decrease of the yield beyond the high energy maximum (Fig.4) occurs for all potassium halides at a photon energy $2E_G+E_{VC}$ /10/. At this energy an excited core electron is just energetic enough to excite a secondary electron from the valence band. The final states of both electrons lie below the vacuum level; this explains the decrease of the yield. The alternative process /10/ in which a highly excited valence electron excites a secondary electron from the core level is much less probable, since the number of unscattered photoelectrons originating from the valence band is negligibly small in this energy range.

3.3 Core Excitons

The prominent doublet in the yield spectra at 20 eV and 21.5 eV (Fig.4) is attributed to core excitons /10/. This interpretation is supported by the fact that the doublet appears for all potassium halides in the optical spectra as well as in the photoyield and its position remains essentially unchanged

when the halide is changed. This suggests that only potassium levels are involved in the corresponding transitions. The bottom of the conduction band is mainly formed by K^+4s-states and its energetic distance from the K^+3p core level has the right magnitude, whereas the valence bands originate essentially from halide states /22/. An argument for the excitonic nature of these peaks is provided by their widths, which are considerably smaller than those of the other maxima in this range. Furthermore, the splitting of about 0.2 eV of the Γ-peak in Fig.4 gives additional evidence. It corresponds to the spin-orbit-splitting of the K^+3p core level. The X-exciton does not show this splitting since its lifetime is shorter because of energetic degeneracy with the conduction band.

In conclusion, there is little doubt that the doublet is due to core excitons. As the final state at least of the Γ-exciton, and in KI also of the X-exciton, lies below the vacuum level, they cannot directly contribute to photoemission. Consequently, a secondary process must be responsible for the core exciton doublet in the photoyield spectrum. The two possible decay processes, direct recombination and Auger process, are outlined in Fig.8. They should produce photoelectrons of different kinetic energy: the electrons originating from the recombination process are energetically indistinguishable from directly excited valence electrons, while the maximum kinetic energy of the Auger electrons is given by $E_{VC}-E_{TH}$. Thus for KI no Auger electron with $E_{kin} > 7.2$ eV can occur. The exciton peaks did

not vanish for retarding potentials above 7.1 eV (cf. Eq.(2) and Table 1) but remained visible up to the stopping potential for unscattered electrons excited from the top of the valence band. This result proves that the direct recombination is at least partly responsible for the exciton doublet.

The question whether or not the Auger process also contributes to the effect can in principle be decided by measuring the peak-to-background ratio as a function of the retarding potential. The minimum kinetic energy of the Auger electrons is given by $E_{VC}-E_{TH}-2E_W$ where E_W denotes the width of the valence band. For KI, E_W=1.5 eV /22/,/24/ and Auger electrons are expected in the energy range 4.2 - 7.2 eV above the vacuum level. Thus an increase of the peak-to-background ratio in this range would give evidence of the Auger process. The situation is complicated, however, by the electron-electron scattering which sets in at 5.3 eV and will strongly reduce the number of Auger electrons above this energy, giving rise at the same time to scattered Auger electrons below 4.2 eV. The experimental data showed a marked increase of the peak-to-background ratio for kinetic energies above 2 eV and a strong decrease above 5 eV. These changes may indicate a contribution of the Auger process, but they do not provide enough evidence to prove it unambiguously.

References

/1/ H.R. Philipp and H. Ehrenreich, Phys.Rev. 131, 2016 (1963)

/2/ M. Watanabe, Y. Nakamura, Y. Nakai, and T. Murata, J.Phys.Soc.Japan 24, 428 (1968)

/3/ D.M. Roessler and W.C. Walker, Phys.Rev. 166, 599 (1968)

/4/ G. Stephan, E. Garignon, and S. Robin, Compt.Rend. 268, 408 (1969); G. Stephan, and S. Robin, Optics Comm. 1, 40 (1969)

/5/ G. Stephan and S. Robin, Compt.Rend. 267 B, 1286 (1968)

/6/ D. Blechschmidt, R. Klucker, and M. Skibowski, phys.stat. sol. 36, 625 (1969)

/7/ P.H. Metzger, J.Phys.Chem.Sol. 26, 1879 (1965)
S.W. Duckett and P.H. Metzger, Phys.Rev. 137, A 953 (1965)

/8/ H. Saito, S. Saito, R. Onaka, and B. Ikeo, J.Phys.Soc. Japan 24, 1095 (1968)

/9/ M. Watanabe, Y. Nakamura, Y. Nakai, and T. Murata, J.Phys.Soc. Japan 26, 1014 (1969)

/10/ D. Blechschmidt, M. Skibowski, and W. Steinmann, Optics Comm. 1, 275 (1970)

/11/ V.S. Fomenko, Handbook of thermoionic properties, New York, Plenum Press 1966

/12/ R.G. Newburgh, Phys.Rev. 132, 1570 (1963)

/13/ J.W. Taylor and P.L. Hartman, Phys.Rev. 113, 1421 (1959)

/14/ H. Philipp, E.A. Taft and L. Apker, Phys.Rev. 120, 49 (1960)

/15/ E.A. Taft and H.R. Philipp, J.Phys.Chem.Solids 3, 1 (1957)

/16/ R.P. Godwin, Springer Tracts in Modern Physics, Vol. 51 (1969)

/17/ R. Haensel and C. Kunz, Z.Angew.Physik 23, 276 (1967)

/18/ M. Skibowski and W. Steinmann, J.Opt.Soc.Am. 57, 112 (1967)

/19/ B. Feuerbacher, M. Skibowski and R.P. Godwin, Rev.Sci. Instr. 40, 305 (1969)

/20/ J.E. Eby, K.J. Teegarden and D.B. Dutton, Phys.Rev. 116, 1099 (1959)

/21/ D. Fröhlich and B. Staginnus, Phys.Rev.Letters 19, 496 (1967)

/22/ Y. Onodera, M. Okazaki, and T. Inoui, J.Phys.Soc. Japan, 21, 2229 (1966)

/23/ K.J. Teegarden and G. Baldini, Phys.Rev. 155, 896 (1967)

/24/ H. Overhof, Verhandl. DPG, 310 (5) 1970

/25/ L.P. Howland, Phys.Rev. 109, 1927 (1958)

/26/ T. Tomiki and T. Miyata, J.Phys.Soc. Japan 27, 658 (1969)

/27/ T. Tomiki, J.Phys.Soc. Japan 22, 463 (1967)

Table 1

	E_G	E_{TH}	E_A	$E_{min}/2$	E_{VC}	$B_V(\Gamma\text{-Ex.})$	$B_C(\Gamma\text{-Ex.})$	Δ	$\Delta-E_G/2$
	1	2	3	4	5	6	7	8	9
KF	10.96 (26) 10.9 (20) 10.8 (23) 10.3 (5)	10.5 10.4 (15)	-0.5 -0.5 (20)	10.7 (10)	10.14 (5)	1.3 (26)		6.4	0.95
KCl	8.7 (27) 8.7 (3) 8.5 (20)	8.9 8.7 (13)	0.2 0.2 (20)	9.10 (10)	12.5 12.4 (6) 12.6 (25)	1.0 0.93 (27)	1.1	5.3	0.95
KBr	7.3 (21) 7.8 (20)	8.0 8.1 (15)	0.7 0.3 (20)	8.25 (10)	13.3 13.3 (6)	0.7	0.7	4.6	0.95
KI	6.3 (21) 6.2 (20)	7.3 7.3 (15) 7.3 (13)	1.0 1.1 (20)	7.3 (10)	14.5 14.6 (6) 15.0 (22)	0.7	0.8	3.15	0.0

Results of this work are listed without reference.

Figure captions

Fig. 1 Sketch of a part of the band structure of KI as calculated by Onodera et al. /22/. Only the lowest part of the conduction band is drawn.

Fig. 2 Potential scheme for the potassium halides with respect to the collector.
CB conduction band, VB valence band
VL vacuum level, E_A electron affinity, E_G gap energy
E_{VC} energy distance between the top of the valence band and the K^+3p core level
E_{FE}, E_{FC} Fermi level of emitter and collector
Δ energy distance between the Fermi level and the top of the valence band
Φ collector work function
U_R retarding potential.

Fig. 3 Stopping potential lines for valence band and K^+3p excitation in KI.

Fig. 4 Spectral distribution of the photocurrent from KI for different retarding potentials.

Fig. 5 Logarithm of the photocurrent from KI for the determination of the onset of K^+3p electrons for different retarding potentials. The arrows indicate the energies at which K^+3p electrons start to contribute to the photocurrent.

Fig. 6 Energy distribution curves of KI for various photon energies in the range 10 - 18 eV. For the abscissa cf. Eq. (1).

Fig. 7 Ratio N_S/N_V of the peak heights of scattered and unscattered electrons as a function of photon energy for all potassium halides.

Fig. 8 Illustration of the recombination and Auger process as secondary processes explaining the excitonic structures in photoemission.

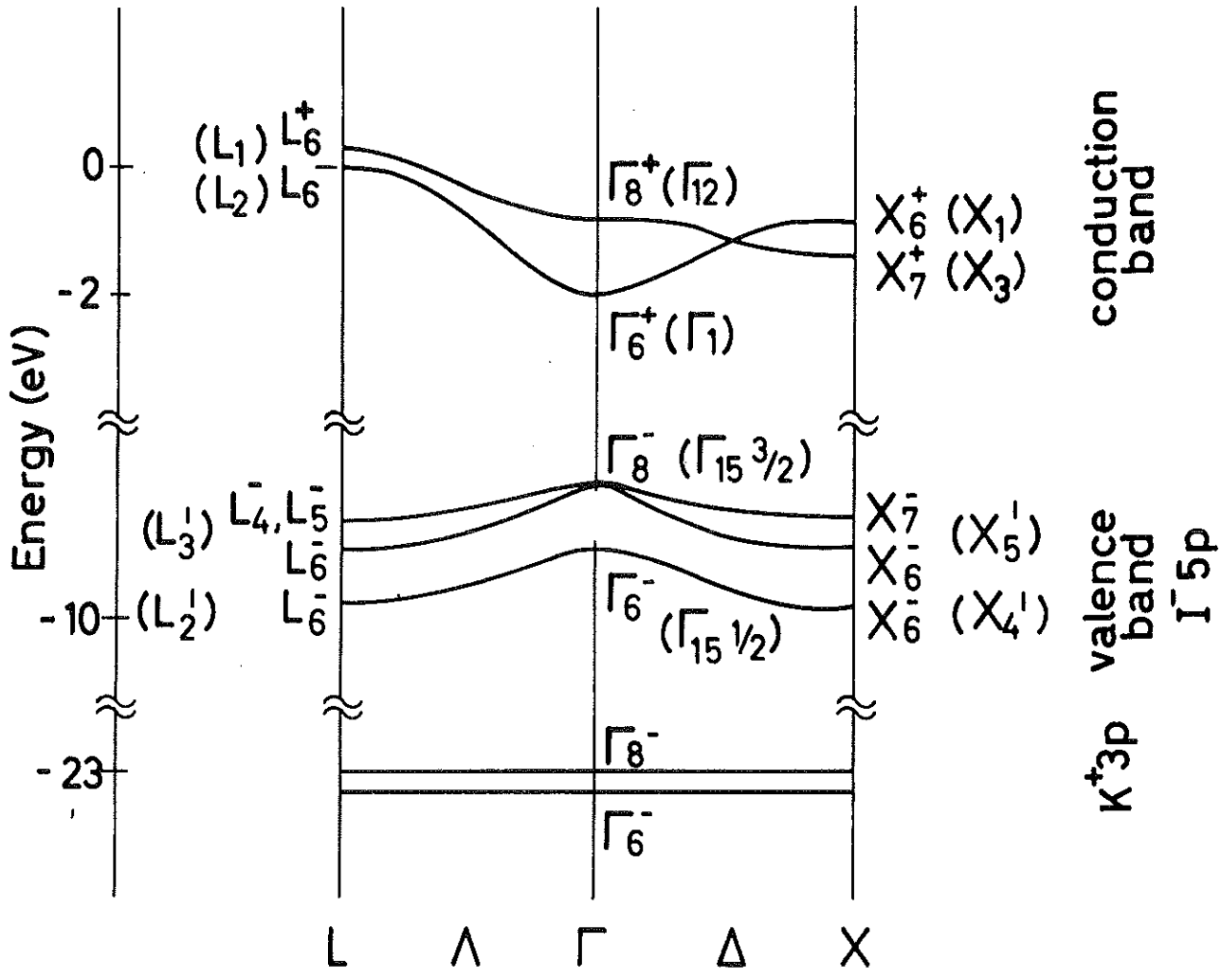
Energy (eV)
0
-2
-10
-23
(L1) L6+
(L2) L6-
(L3') L4-, L5-
L6-
(L2') L6-
Γ8+ (Γ12)
Γ6+ (Γ1)
Γ8- (Γ15 3/2)
Γ6- (Γ15 1/2)
Γ8-
Γ6-
X6+ (X1)
X7+ (X3)
X7- (X5')
X6-
X6- (X4')
conduction band
valence band
K+3p
I-5p
L
Λ
Γ
Δ
X

Fig.1

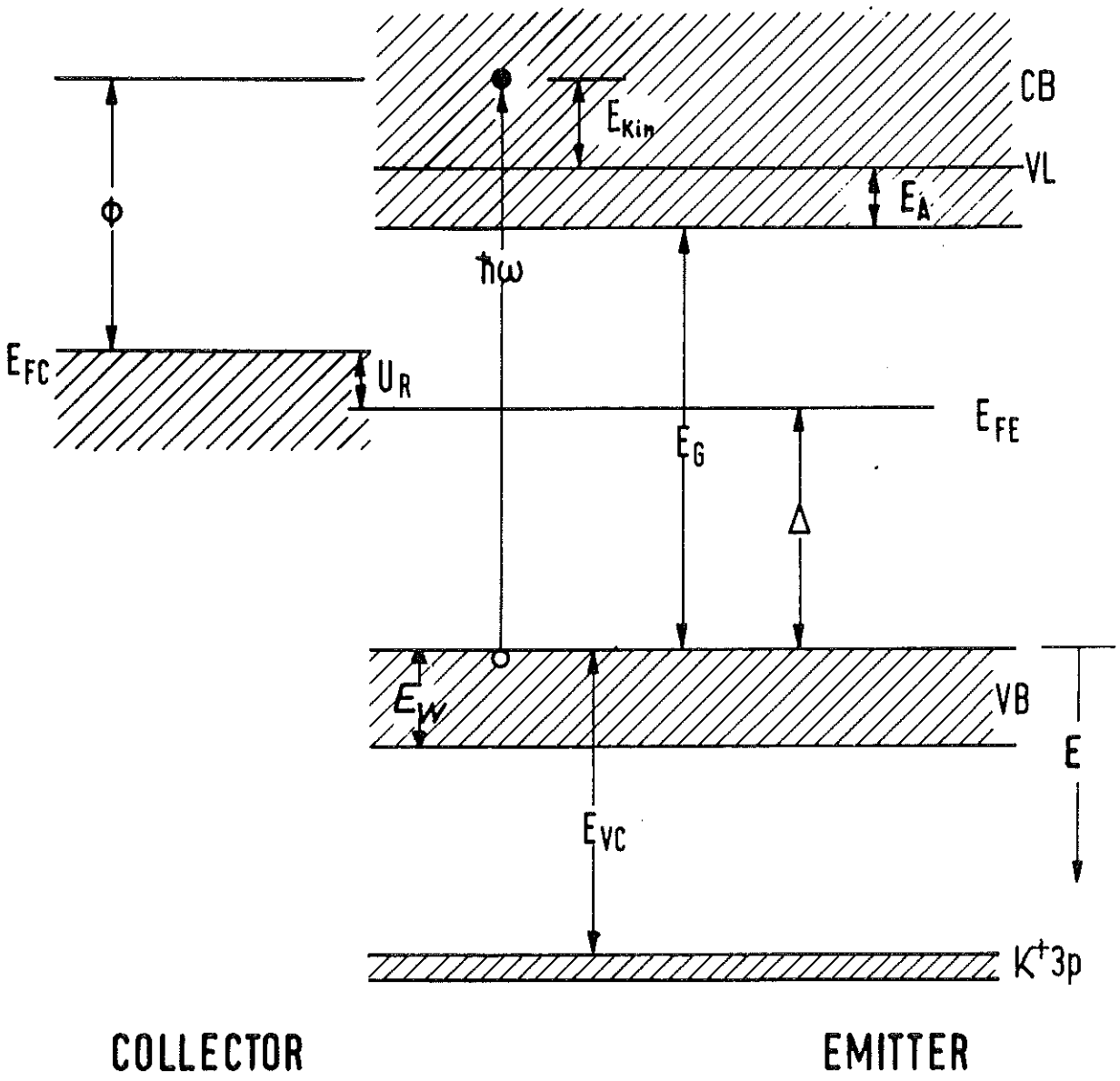
CB
VL
E_{Kin}
E_A
Φ
$\hbar\omega$
E_{FC}
U_R
E_{FE}
E_G
Δ
VB
E_W
E
E_{VC}
K^+3p
COLLECTOR
EMITTER

Fig.2

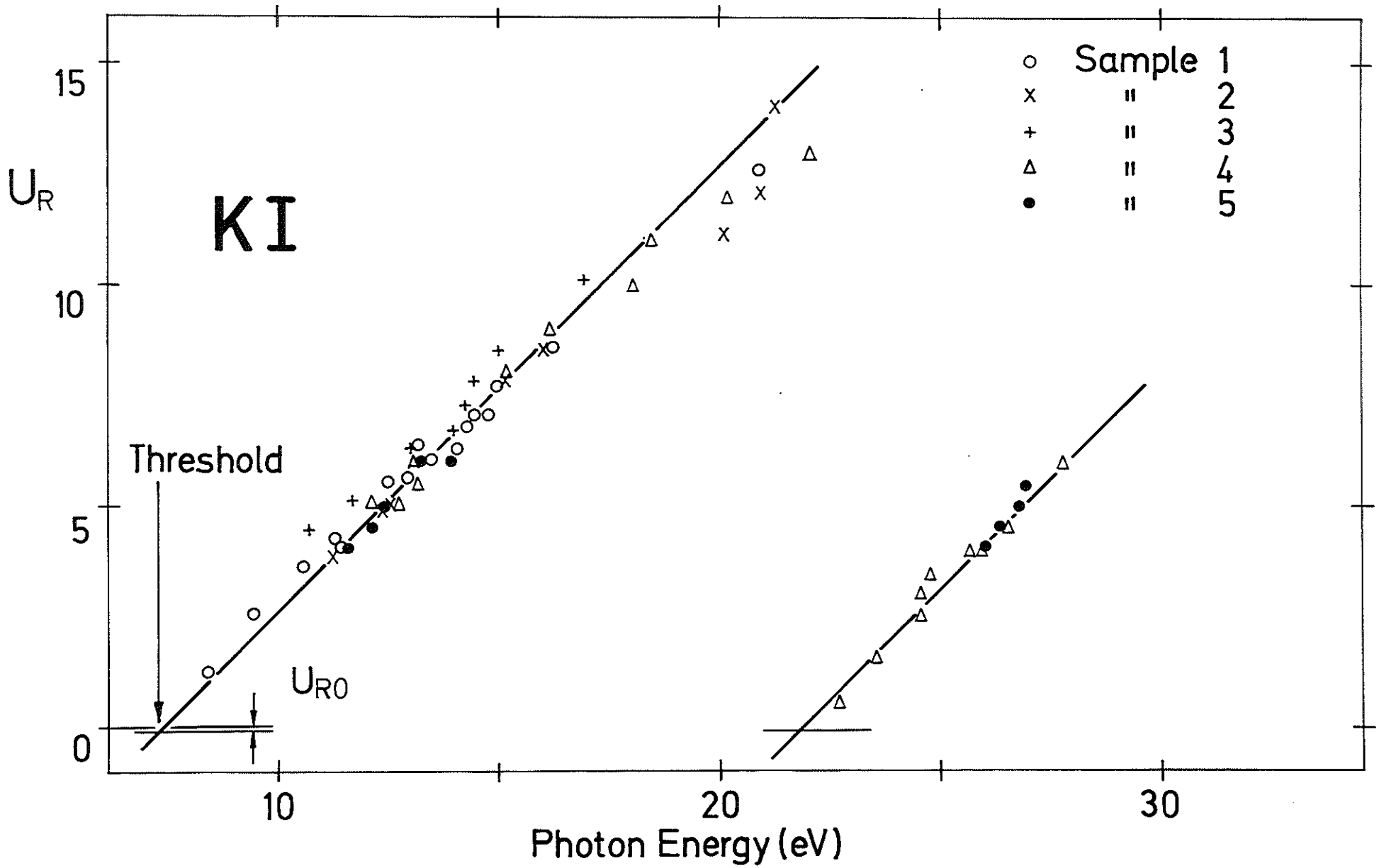
KI
Sample 1
2
3
4
5
Threshold
U_{R0}
U_R
15
10
5
0
10
20
30
Photon Energy (eV)

Fig.3

KI
$2E_G$
$2E_G+E_{VC}$
E_{TH}
Γ
X
-20.0
-1.0
0.0
+0.5
+1.0
+1.5
+2.0
+2.5
+3.0
+3.5
Photocurrent (arbitrary units)
Photon Energy (eV)
5
10
15
20
25
30

Fig.4

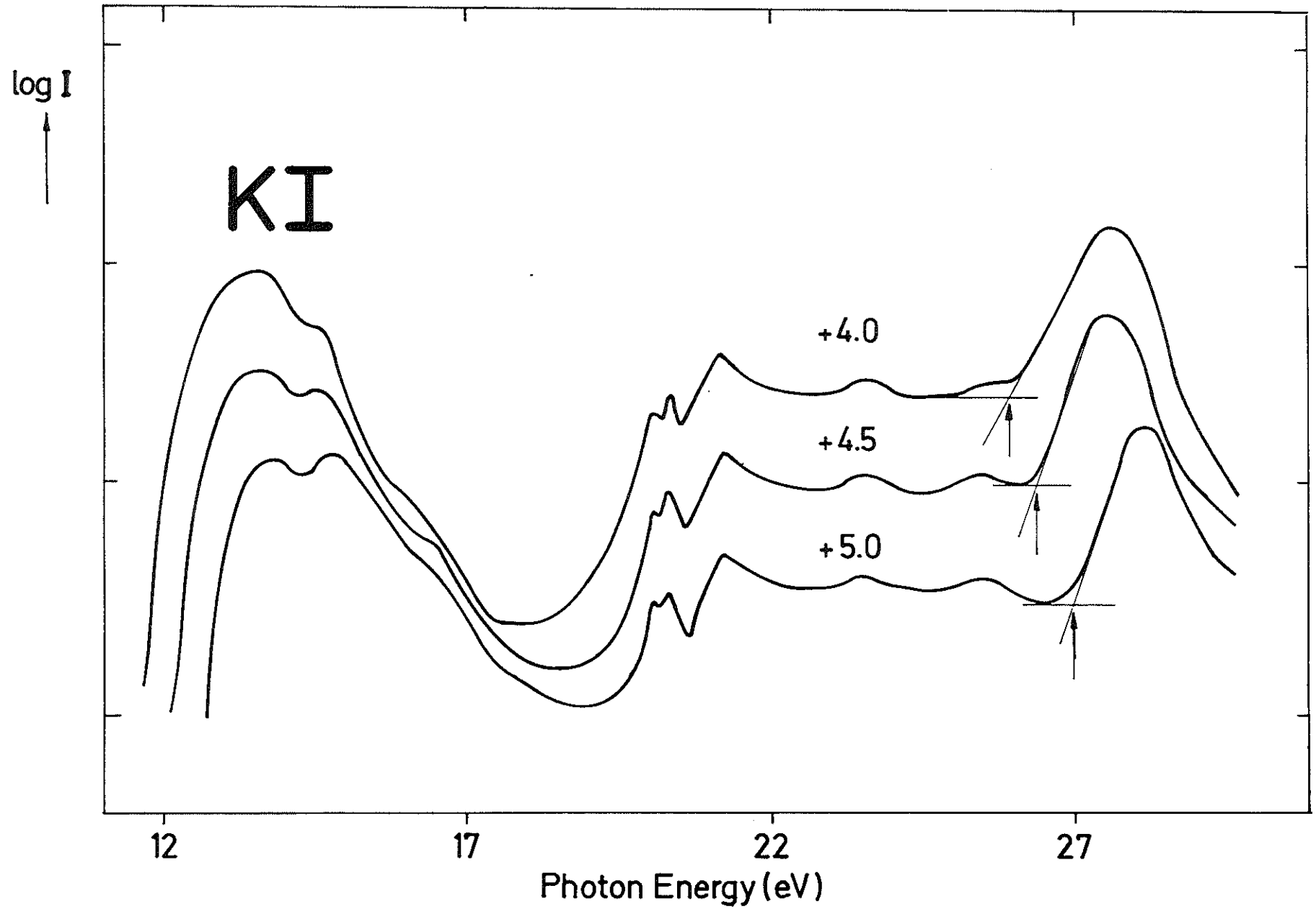

Fig.5

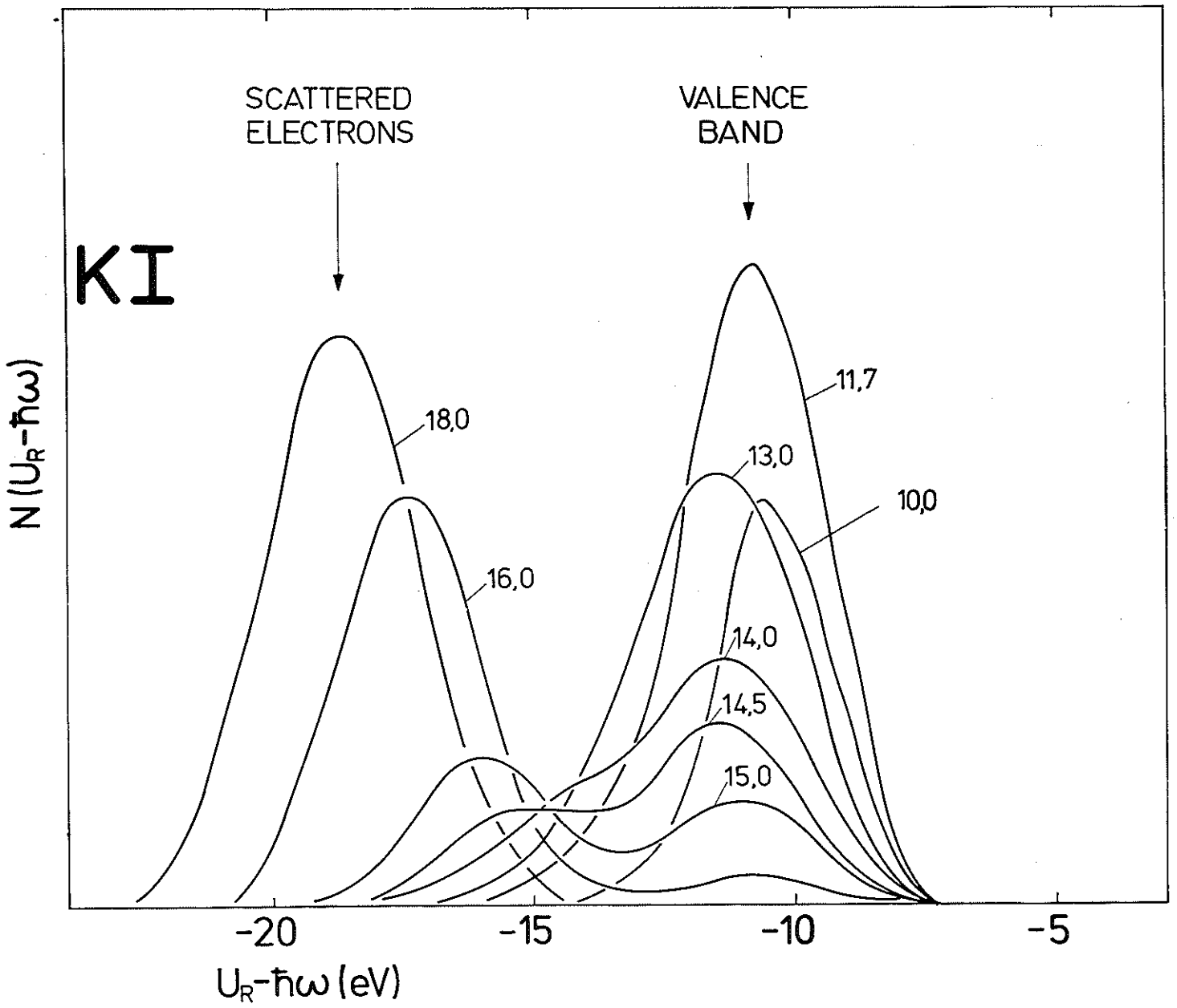
SCATTERED
ELECTRONS
VALENCE
BAND
KI
18,0
16,0
11,7
13,0
10,0
14,0
14,5
15,0
N (U_R-ħω)
-20
-15
-10
-5
U_R-ħω (eV)

Fig.6

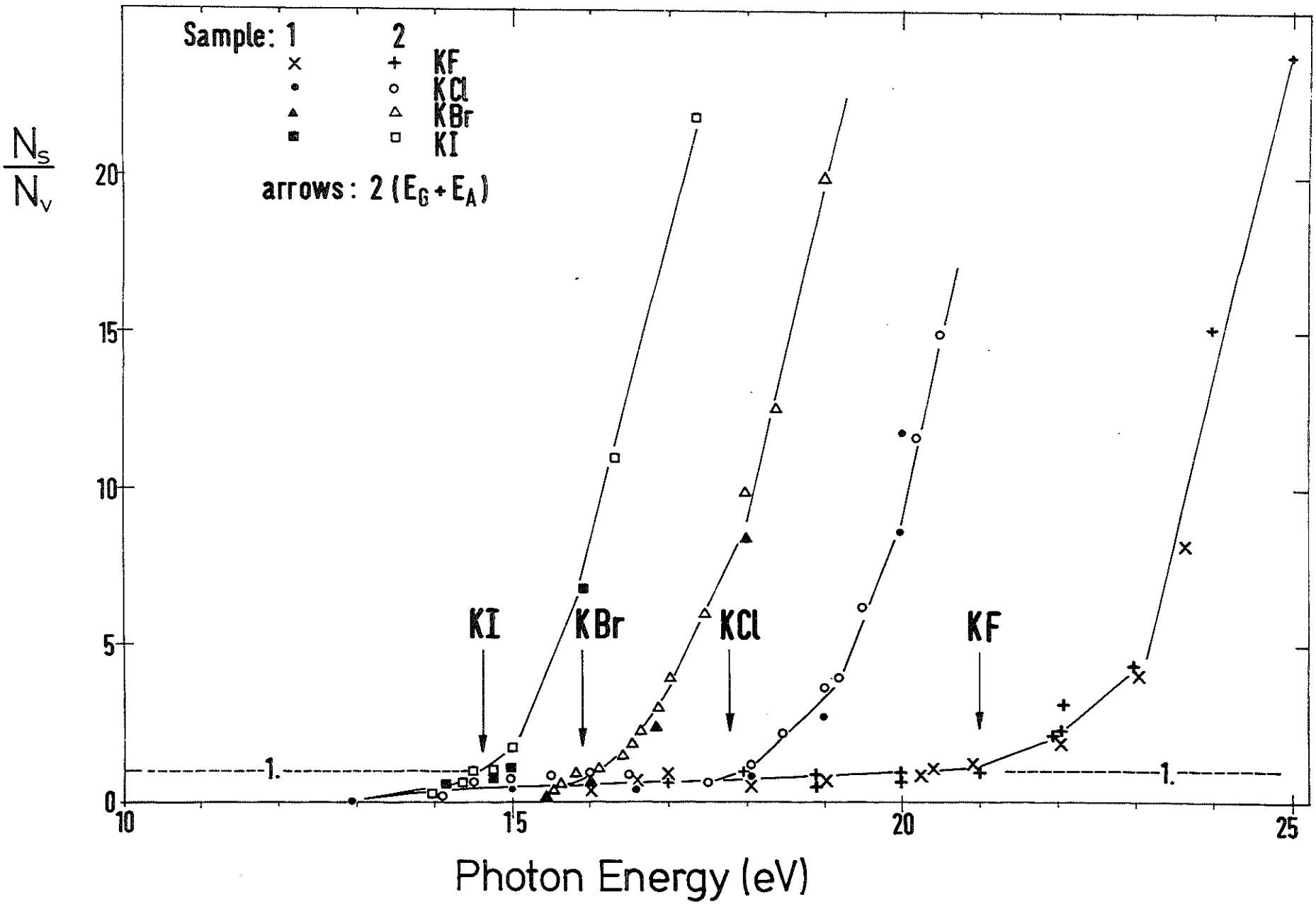
Sample: 1 2
KF
KCl
KBr
KI
arrows: 2 (E_G + E_A)
N_s / N_v
20
15
10
5
0
1.
1.
KI
KBr
KCl
KF
10
15
20
25
Photon Energy (eV)

Fig. 7

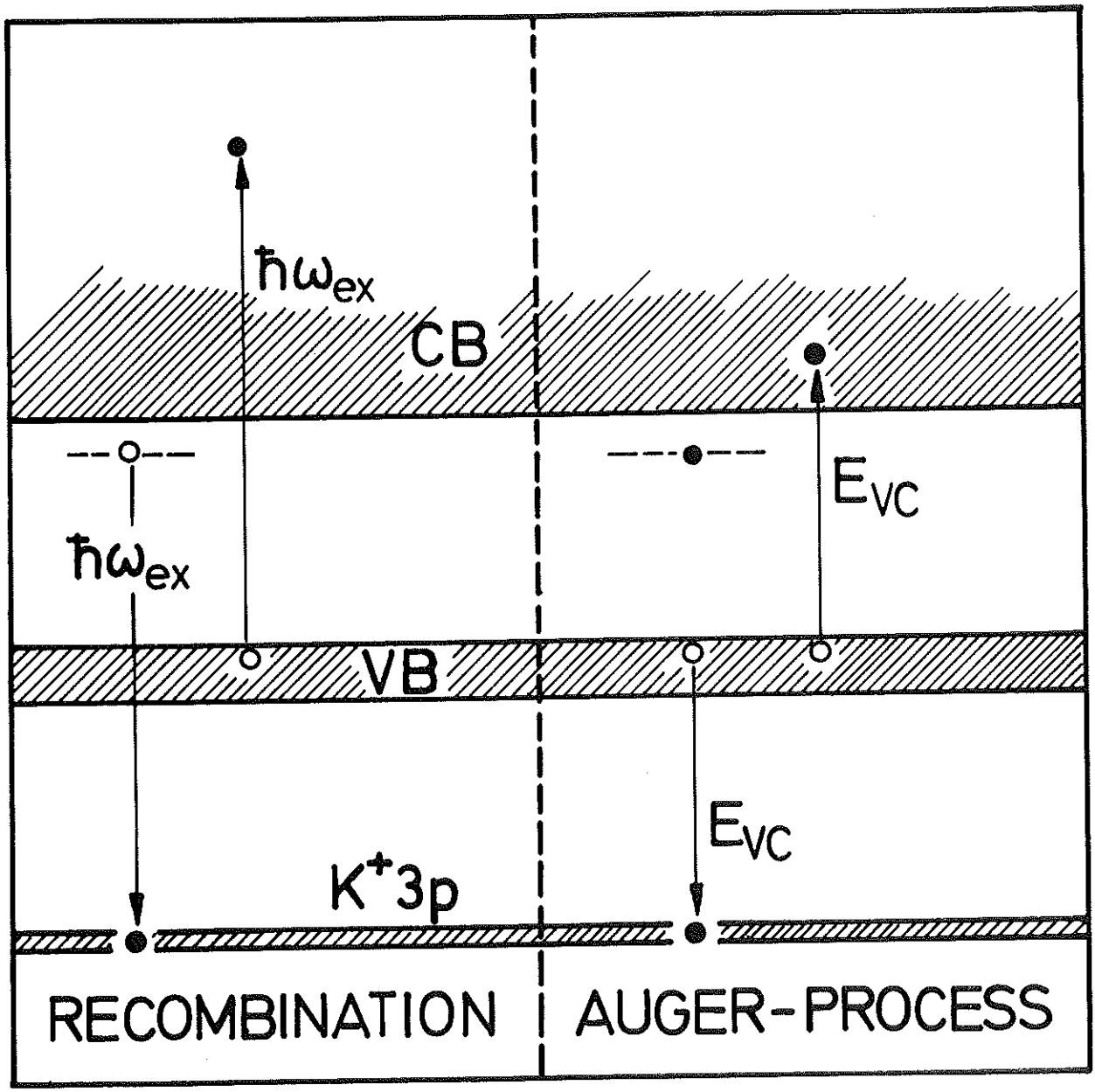

Fig.8